



Effects of loading rates on mechanical property and failure behavior of single-lap adhesive joints with carbon fiber reinforced plastics and aluminum alloys

Shaoluo Wang¹ · Wei Liang¹ · Liming Duan¹ · Guangyao Li¹ · Junjia Cui¹

Received: 21 September 2019 / Accepted: 3 December 2019 / Published online: 23 December 2019
© Springer-Verlag London Ltd., part of Springer Nature 2019

Abstract

In this paper, the effects of loading rate on mechanical property and failure mode of carbon fiber reinforced plastic (CFRP) composite and aluminum alloy (Al) single-lap adhesive joints were investigated. Four loading rates (2 mm/min, 4 m/s, 8 m/s, and 12 m/s) were chosen to carry out the shear tests. Digital image correlation (DIC) technique was used to analyze the strain evolution of the joints. Results showed that the shear strength increased with the increase of loading rate. When the loading rate increased from 2 mm/min to 12 m/s, the average shear strength of the joint increased from 19.3 to 29.2 MPa. The load-displacement curves under dynamic loading had two peaks, which is mainly caused by local failure and progressive failure of the joints. There were stress concentrations at both ends of the bonding area, which caused cohesive failure and fiber-tear failure. At both ends of the bonding area, the failure mode was mainly cohesive failure of the adhesive, whereas the failure mode in the middle of the bonding area was mainly resin matrix failure of the CFRP. Wherein the peak loads had a certain correspondence with failure modes and failure regions.

Keywords CFRP/aluminum adhesive joints · Bonding process · High loading rates · Failure behavior and mechanism

1 Introduction

Considering the light-weight, high-strength, anti-corrosion, and crashworthiness, the mixed uses of carbon fiber-reinforced plastic (CFRP) composite and aluminum alloy (Al) have become a trend in vehicle components and aerospace structures [1–7]. The joining methods of CFRP/CFRP or CFRP/Al mainly consist of riveting, bolted connection and adhesive bonding. The riveting and the bolted joining require pre-manufactured holes, which will lead to stress concentration on the joining part or a strength reduction of the CFRP plate. Thus, adhesive bonding has gained extensive attention to join dissimilar materials, especially CFRP and Al, for its relatively low stress concentration, high fatigue resistance, corrosion resistance, good sealing performance, and reservation of structural integrity [8–12].

In the automotive and aerospace industries, adhesive joints are often subjected to impact loading during the fabrication or service. The impact loading has a great influence on the mechanical property and failure behavior of the adhesive joints. Hence, it is necessary to study shear strength and failure mode of the adhesive joints at various loading rates [13]. A systematic study on mechanical behavior of the CFRP/CFRP single-lap adhesive joints at different loading rates (1 mm/min–2 m/s) was conducted by Araújo et al. [14]. They found that the failure load under impact was evidently higher and the failure followed the cohesive mode in adhesive and delamination mode in CFRP. They speculated that this phenomenon was due to strain rate sensitivity of adhesive and CFRP resin. The performance of CFRP/CFRP and CFRP/Al single-lap adhesive joints at quasi-static and impact conditions (1 mm/min–3 m/s) was performed by Machado et al. [15, 16]. All the adhesive single-lap joints tested were found to exhibit strain rate dependency. Srivastava et al. [17] researched the effect of loading rates on shear strength of the single-lap adhesive joints. Results showed that the shear strength of the joints increased when the loading rate increased. The axial residual properties of the CFRP/Al single-lap adhesive joints under different strain rates (1.3 mm/min–5 m/s) after low-velocity

✉ Junjia Cui
cuijunjia@hnu.edu.cn

¹ State Key Laboratory of Advanced Design and Manufacturing for Vehicle Body, Hunan University, Changsha 410082, China

transverse pre-impact were studied by Liu et al. [18]. They found that the joint strength showed a rising tendency with increasing strain rate, and the failure mode of the adhesive joints transformed from the cohesive and adhesive failure to the cohesive and fiber-tear failure.

Although dynamic behavior and failure mode of the adhesive joints have been studied by some scholars, they are not systematic and in-depth. Especially, the effect of dynamic loading rates on microscopic failure mechanism of the CFRP/Al single-lap adhesive joints has not been fully and systematically investigated.

In this work, the aim was to investigate the effects of dynamic loading rates (2 mm/min–12 m/s) on mechanical property and failure behavior of the CFRP/Al single-lap adhesive joints. The failure process was recorded by means of a high-speed camera. In order to analyze the full field strain distribution of the joint, the digital image correlation (DIC) technique was adopted. In addition, the microstructure morphology of the failure surface was observed by scanning electron microscope (SEM). Based on the test results, the reasons for the difference of the joint performance at various loading rates were analyzed.

2 Experimental

2.1 Materials

In this study, the CFRP composite laminate, the aluminum alloy 5182 (Al5182) and the epoxy adhesives were used in the CFRP/Al5182 adhesive single-lap joints. The properties of CFRP composite laminate are presented in Table 1. The matrix in the CFRP laminate was epoxy resin. The material parameters of Al5182 plate and adhesive are showed in Tables 2 and 3, respectively.

2.2 Specimen preparation

The CFRP and Al5182 plate were cut into the size of 25 mm × 100 mm (W×L), and the dimensions of CFRP/Al5182 single-lap adhesive joints were designed according to ISO 4587 standard [19] as shown in Fig. 1. The thickness of CFRP and Al5182 plate were 2.5 mm and 1.8 mm, respectively. The size of bonding area was 25 mm × 12.5 mm (W×L) and the thickness of the adhesives was 0.2 mm. It should be pointed out that

the thickness (D) of the adhesives had considerable effects on the bond strength and failure mode [20]. Thus, it was very important to ensure that the adhesive thickness of all the specimens was consistent. A shim of certain thickness (herein was 2 and 2.7 mm) was used to ensure the thickness of the adhesives.

According to report [21], the surface treatment had a significant effect on bonding performance. The performance of the joints without surface treatment was unsatisfactory in the previous study. Hence, emery clothes of P360 were used to polish the surface of CFRP and Al5182 plates in order to improve the performance of the joints. Then, the surface was cleaned after being polished.

A thermostatic drying oven was used in the curing process. During the curing process, the viscosity of the adhesive would decrease. The Al plates would also move slightly due to thermal expansion. Thus, the specimens needed to be fixed to ensure the sizes of the bonding area.

The process of specimen preparation was as follows: first, emery clothes were used to polish the surface of the CFRP/Al plates. Then the plates were cleaned and the adhesives were evenly daubed on the joining area of CFRP/Al plates. Two plates (CFRP/Al5182) were aligned and lapped together, and the shims and fixtures were used to ensure the thickness of the adhesives. Finally, the adhesive joints were cured in a thermostatic drying oven at 180 °C for 2 h.

2.3 Principles and apparatuses of the test

To investigate the effect of high loading rate on the CFRP/Al5182 adhesive single-lap joints, four loading rates were selected in the shear tests (one for quasi-static shear test, 2 mm/min, and three for high-speed shear tests, 4 m/s, 8 m/s, 12 m/s). Five repeated trials were carried out under each loading rate. All the tests were performed at room temperature (25 °C). The shear strength is given by Eq. (1).

$$\tau = F/(BL) \quad (1)$$

Where τ is the shear strength, F is the tensile load, B is the width of the joint, and L is the length of the overlap.

Quasi-static shear tests were implemented with the universal testing machine. High-speed shear tests were conducted with the high-speed testing machine. The loading rate range of the high-speed testing machine is 0.001 m/s–20 m/s, and the maximum loading force can reach to 50 kN.

Table 1 Properties of CFRP composite laminate

Brand	Fiber strength (MPa)	Fiber modulus (GPa)	Resin volume fraction	Tensile strength (MPa)	Tensile modulus (GPa)	Layer number	ply orientation
T300	3530	230	40%	911	76	17	0°, 90°

Table 2 Material parameters of A15182 plate

Density (kg/m ³)	Young's modulus (GPa)	Yield strength (MPa)	Poisson's ratio	A15182 plate thickness (mm)
2560	70	150	0.33	1.8

The DIC technique was used to analyze the strain distribution of the joints during the shear tests. The surfaces of A15182 plates were chosen in the DIC analysis. The strain field of the surface could represent the strain distribution of the bonding area. The failure process was observed and recorded by the high-speed camera. The strain was calculated by the commercial DIC software (Vic-2D 6) through tracking the movement of the speckle (the movement of each pixel) from initial images to deformed images. The layout patterns of high-speed test system are shown in Fig. 2. The failure surfaces were observed by the scanning electron microscope (SEM).

3 Result and discussion

3.1 Mechanical performance analysis and failure stages division

Figure 3 shows the typical shear load-displacement curves of the CFRP/A15182 adhesive single-lap joints. From Fig. 3(a), the curves under quasi-static and high-speed shearing were significantly different. During the quasi-static shearing tests, the shear load kept increasing until the joints failed accompanied by slight fluctuations. However, the curves during the high-speed shearing exhibited greater fluctuations. The fluctuations might be generated by the micro-crack propagation and the local progressive failure of the joints. The difference of fluctuations degree between high-speed and quasi-static curves was mainly caused by the loading rate effect of the adherends and the time and sufficiency of micro-crack propagation. Moreover, the failure load of the joint at quasi-static was lower than that at high-speed, and the failure load of the joint elevated with the increase of loading rate.

Both high-speed and quasi-static shearing process could be divided into three stages as shown in Fig. 3(b) and (c): (I) the loading stage (the load kept rising and the adherends began to deform); (II) the wavy stage (the curves fluctuated since the cracks generated and extended in the bonding area); (III) the joint failure stage (the softening region with the catastrophic fracture).

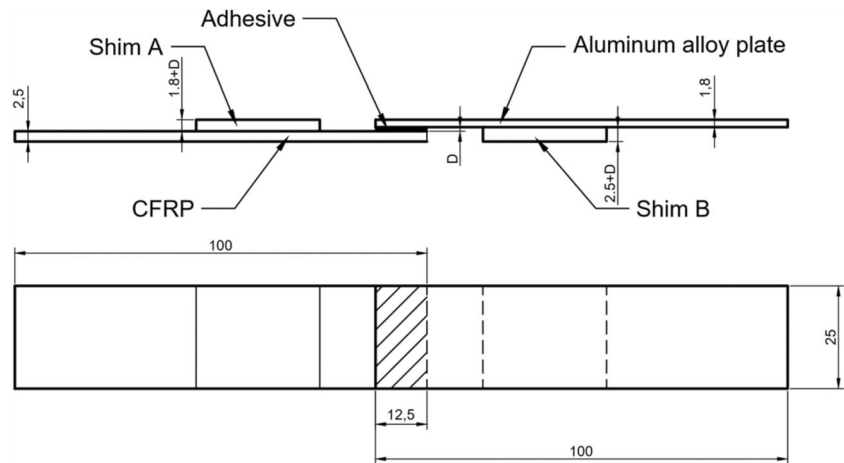
It could be observed that the curves of the high-speed shearing tests had two peaks during the failure process. The peaks were marked as Peak A and Peak B as shown in Fig. 3(b). The average value of the Peak A and Peak B at different loading rates are presented in Table 4. The value of Peak A was smaller than that of Peak B. Peak B was relatively more affected by loading rate than the Peak A. At the loading stage (I), the joint began to deform while the loading force rose. The micro-cracks were generated in the adhesive and the CFRP resin matrix, and the load was decreased to enter the stage of load fluctuations. At the wavy stage (II), the shear load went down first and then went up to Peak B. This phenomenon was mainly caused by local failure and progressive failure of the joints. From the failure behavior analysis (in Section 3.2) below, it was known that the failure mode of the joints had also changed in this process. During the high-speed shearing tests, the failure of the joints was not completed in an instant. Because the A15182 plate would undergo large deformation, the micro-cracks were more likely to occur in the deformed area, resulting in local failure. The local failure occurred before catastrophic failure, and the failure mode of the joints had changed simultaneously. Hence, the load was temporarily decreased on account of the transition of the failure mode in the joints. Nevertheless, the joints were still able to withstand larger load. The load rose again until the joint finally failed. At the joint failure stage (III), the cracks propagated quickly after Peak B and the shear load went down. The Peak B was the maximum load that the joint could withstand, which represented the shear strength of the joint.

The average shear strength of the CFRP/A15182 single-lap adhesive joints under different loading rates are illustrated in Fig. 4. It could be observed that the joint shear strength increased with the increase of loading rate. Compared with the quasi-static condition (2 mm/min), the shear strength of the joints at dynamic loading rate of 4 m/s, 8 m/s, and 12 m/s had increased 14.29%, 41.82%, and 51.19%, respectively. One of the reasons for this phenomenon was the difference in the time and sufficiency of the micro-crack propagation of the joint under various loading rates. Figure 5 shows the shear load-time curves of the shearing tests. The shear

Table 3 Material parameters of adhesives

Curing temperature (°C)	Curing time (min)	Density (kg/m ³)	Young's modulus (GPa)	Poisson's ratio
180	120	1300	2.20	0.36

Fig. 1 Geometry and dimensions of the single-lap joint specimens (Unit: mm)



process lasted for less than 1 ms in the high-speed shearing tests. However, in the quasi-static shearing tests, the shear process lasted for more than 40 s, much longer than the high-speed shearing tests. For the selected four loading rates, the fracture time of the joints decreased with the increase of loading rate. And the ratio of the fracture time of two loading rates was approximately equal to the inverse ratio of the corresponding loading rate. The shear duration would affect the propagation of micro-cracks in the failure process of the joint. When the loading rate was low, the loading and failure process of the joint was longer. After the micro-cracks were generated, they had more time to extend within adhesive, bonding interface or CFRP resin matrix. Full extension of the micro-cracks reduced the maximum load that the joint could withstand and the shear strength decreased. Under conditions of high-speed shearing, since failure process of the joints lasted for a very short time, the micro-cracks were not fully extended, so that the joint had a higher strength and could bear a higher shear load.

In addition, there were many other factors that contribute to the difference in shear strength of the joint at different loading rates. The difference in stiffness of the joint at different loading rates was also one of the reasons of this phenomenon. The stiffness of the CFRP/A15182 adhesive single-lap joints under different loading rates are illustrated in Fig. 6(a). It could be observed that the joint stiffness increased with the increase of loading rate. Compared with the quasi-static condition (2 mm/min), the stiffness of the joints at dynamic loading rate of 4 m/s, 8 m/s, and 12 m/s had increased 85.5%, 94%, and 96.7%, respectively. The joint was strengthened in high speed and the joint stiffness was also significantly increased, which made the adherends less susceptible to warping during tensile deformation process. Hence, the deformation of the adherends was reduced, and the peeling stress of the joint during the shearing process became smaller. In this case, the shear resistance of the joint was good and the peeling resistance was poor. In other words, the reduction of the deformation of the adherends was beneficial to reduce the peeling stress during

Fig. 2 The layout patterns of the test system

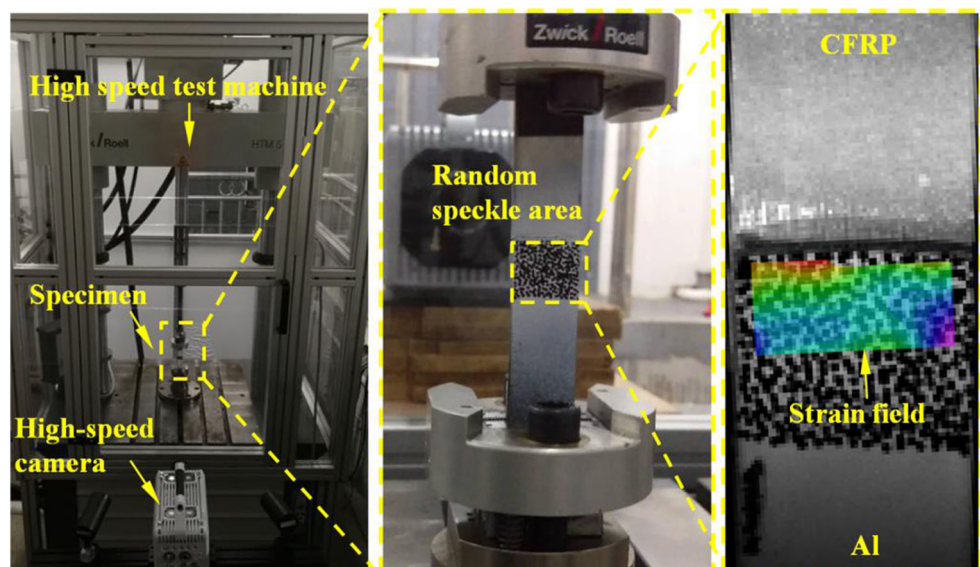
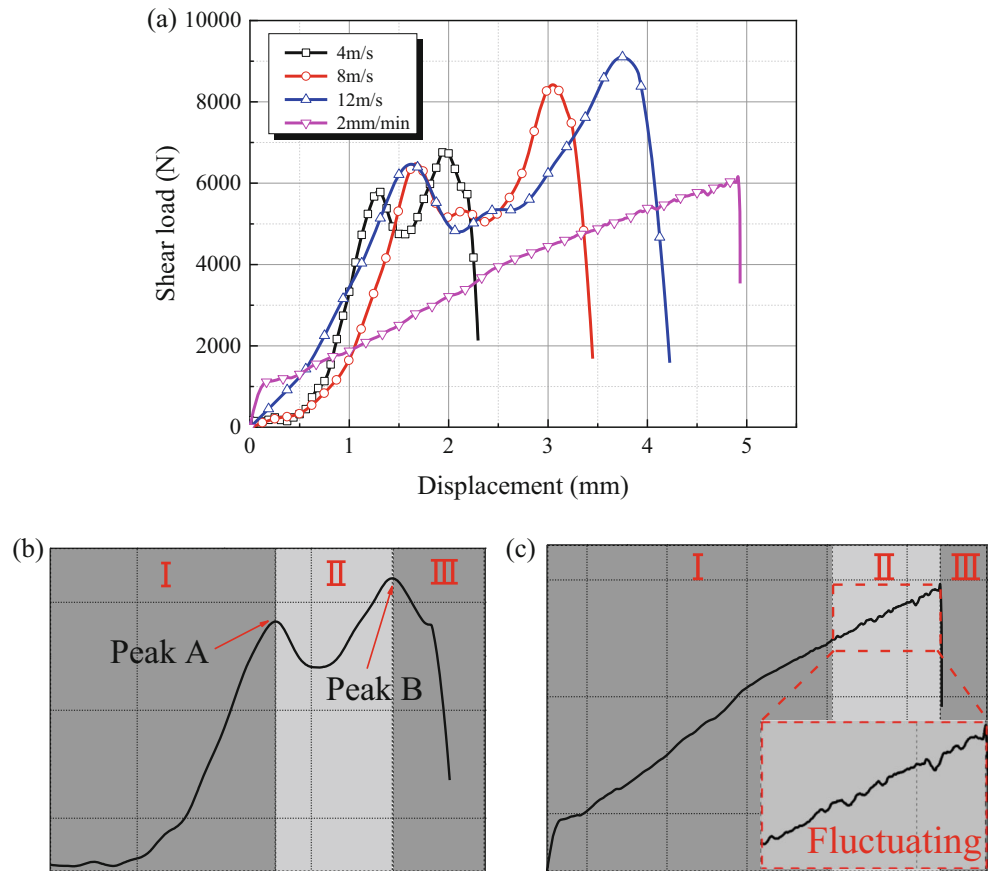


Fig. 3 Typical shear load-displacement curves of the CFRP/Al5182 adhesive joints: **a** at different loading rates; **b** the stage division of the curves in high-speed shearing tests; **c** the stage division of the curves in quasi-static shearing tests



the joint shearing process and thus to improve the joint strength [22, 23].

During the shearing tests, the joint needed to absorb energy until reaching the failure energy to make the joint failure. As the loading rate was increased, the duration of the joint failure process was greatly shortened, and the load of the joint rose rapidly to reach the failure energy in a shorter time, thus the joint failure load was higher in the high-speed shearing tests. The average elongation of the Al5182 plate of the joints under different loading rates is shown in Fig. 6(b). The Al5182 plate of the joints had plastic deformation in all shearing tests. In the quasi-static shearing tests (2 mm/min), there was a large elongation as the joint had a long duration of plastic deformation. However, in the high-speed shearing tests, due to the short duration of the shearing process, the joint had been broken

in the early stage of plastic deformation of Al5182 plate, and the elongation was much lower than that of the quasi-static shearing. A smaller amount of elongation meant that the adherends absorbed less energy in the loading stage. Therefore, more energy needed to be absorbed when the joint eventually failed.

Table 4 The average of Peak A and Peak B at dynamic loading rates

Loading rate (m/s)	The value of Peak A (N)	The value of Peak B (N)
4	5854.44	6907.88
8	6531.65	8488.05
12	6581.82	9165.27

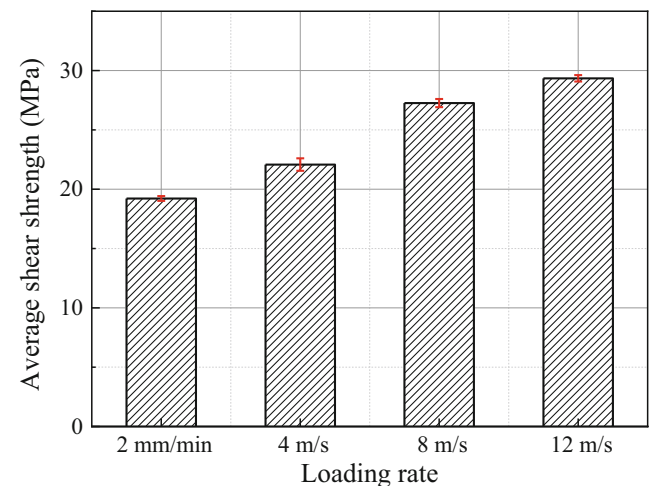


Fig. 4 The average shear strength of the CFRP/Al5182 single-lap adhesive joints under different loading rates

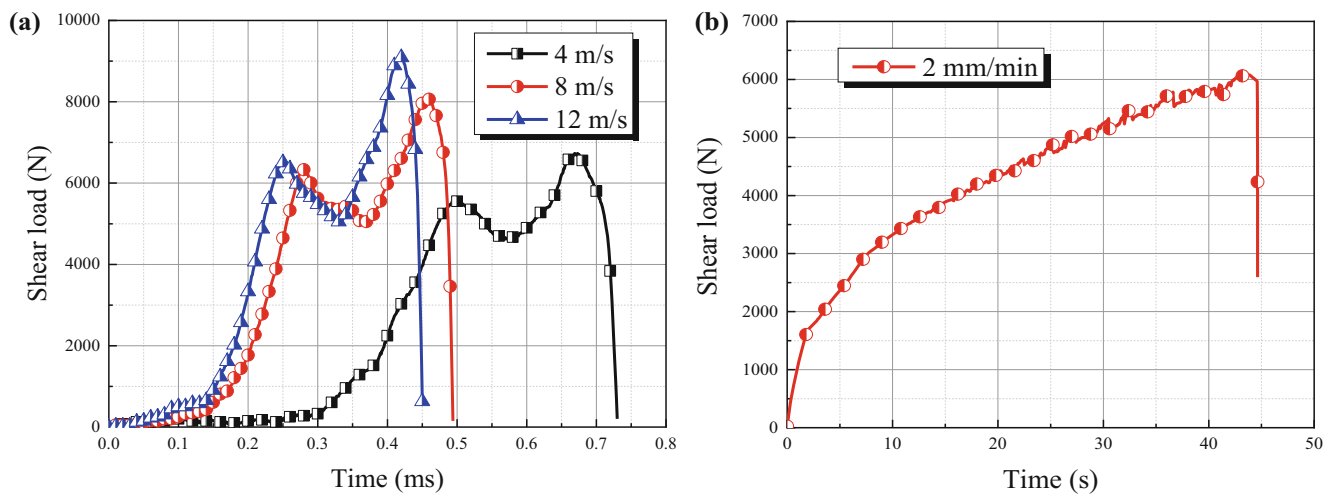


Fig. 5 Shear load-time curves of the CFRP/Al5182 single-lap adhesive joints under different loading rates: **a** in high-speed tests; **b** in quasi-static tests

3.2 Failure behavior analysis

The failure behavior of the CFRP/Al5182 single-lap adhesive joints could be divided into several types: the adhesive failure, the cohesive failure, the CFRP failure, the adherend break failure, and the mixed failure [24]. Adhesive failure represented that the debonding failure occurred on the interface between adhesive and adherends. Cohesive failure represented that the failure occurred inside the adhesive. The CFRP failure included resin matrix failure (the surface of CFRP peeled off) and fiber-tear failure, which represented that the failure occurred in the CFRP plate. The mixed failure included two or more of the abovementioned various failure modes.

In this study, the failure behavior of the CFRP/Al5182 adhesive single-lap joints was mainly cohesive failure (A), fiber-tear failure (B), and resin matrix failure (C) as shown in Fig. 7. The failure behavior at both ends of the bonding area was mainly cohesive failure. The cohesive failure

occurred due to high stress concentrations at both ends of the overlapping area. Close to this area, there was a small region of cohesive failure and fiber-tear failure mixed failure behavior. Wherein, carbon fibers were sheared and broken from the edge of the area. Nevertheless, the failure behavior in the middle of the bonding area was mainly resin matrix failure. Because the stress distribution in the middle of the bonding area was uniform, the failure behavior was dominated by resin matrix failure. Simultaneously, it indicated that the strength of the adhesive had reached or exceeded the strength of the CFRP resin matrix.

The observation points (1, 2, 3) and microstructure morphology of the failure surface were clearly observed by SEM micrographs as shown in Fig. 8(a) and (b). It could be evidently seen that the cohesive failure and the fiber-tear failure occurred at the both ends (1, 3) of the bonding area. Whereas, at the middle of the bonding area, the carbon fiber-tear failure rarely occurred, the failure mode was mainly the CFRP resin

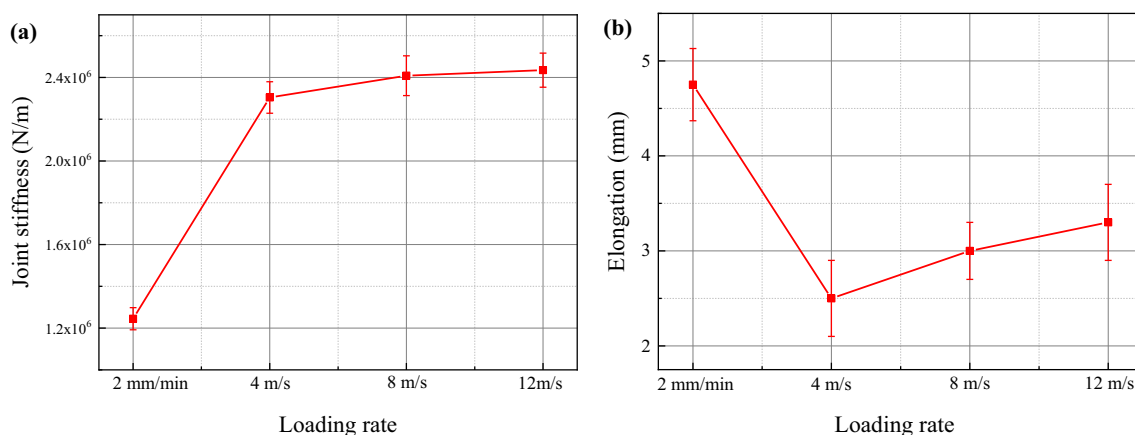


Fig. 6 The stiffness and elongation of the CFRP/Al5182 single-lap adhesive joints under different loading rates: **a** joint stiffness; **b** average elongation of the joints

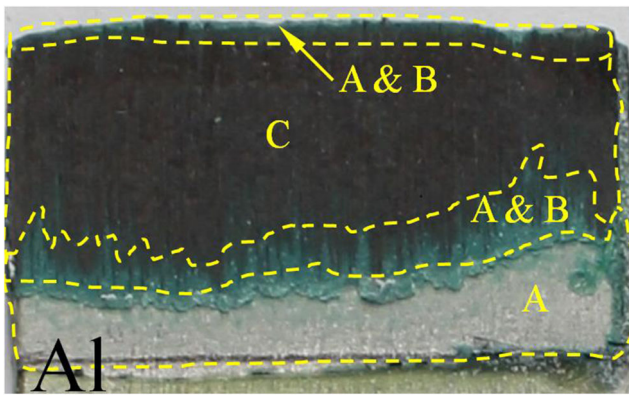


Fig. 7 The failure behavior mode of the CFRP/Al5182 adhesive single-lap joints: A. cohesive failure; B. fiber-tear failure; C. resin matrix failure

matrix failure. Therefore, the failure mode was mainly cohesive failure and fiber-tear failure in both areas of 1 and 3, and the failure mode was mainly resin matrix failure in the area of 2. But the fiber-tear failure mainly occurred at the junction of the cohesive failure and the resin matrix failure.

Furthermore, it could be found that the failed resin matrix exhibited a jagged edge failure surface. And the jagged edges were always slanted to the shearing direction of the adherends as shown in Fig. 9. This showed that the cracks did not spread in straight lines, the crack propagation process had undergone countless repeated processes. Within each individual

propagation process, the cracks propagated at an angle close to 45° to the largest diameter of the carbon fiber. Due to the limitation of the structure, they could propagate transversely rather than further downward under the influence of tensile force, and then entered the next cycle.

To compare and analyze the differences of the failure behavior modes at various loading rates, the failure surfaces (the bonding areas) were divided into three regions as shown in Fig. 10. At the bonding area near the side of Al5182 plate, there was a large amount of adhesive cohesive failure area, which was Region 1. At the bonding area close to the side of CFRP plate, there was a small amount of adhesive cohesive failure area, which was Region 3. The middle area was mainly the area of the CFRP resin matrix failure, which was Region 2. Region 1, Region 2, and Region 3 were on Al5182 plate. The corresponding areas on CFRP plate were Region 1', Region 2', and Region 3', respectively. Region 1 and Region 1' were the same areas on different substrates (the Al5182 and CFRP plate). At the same loading rate, both Region 1 and Region 3 were mainly cohesive failure of the adhesive, but their proportion was significantly different. The area of Region 1 was significantly larger than the area of Region 3. The asymmetry of the distribution of the residual adhesive revealed that the generation and propagation of the cracks in the joints were also asymmetrical. As shown in Table 5, the area proportion of Region 1 was different at various loading rates. In the high-speed shearing tests, the

Fig. 8 Observation points and microstructures of the failure surface: **a** the selected observation points (1, 2, 3); **b** the microstructure

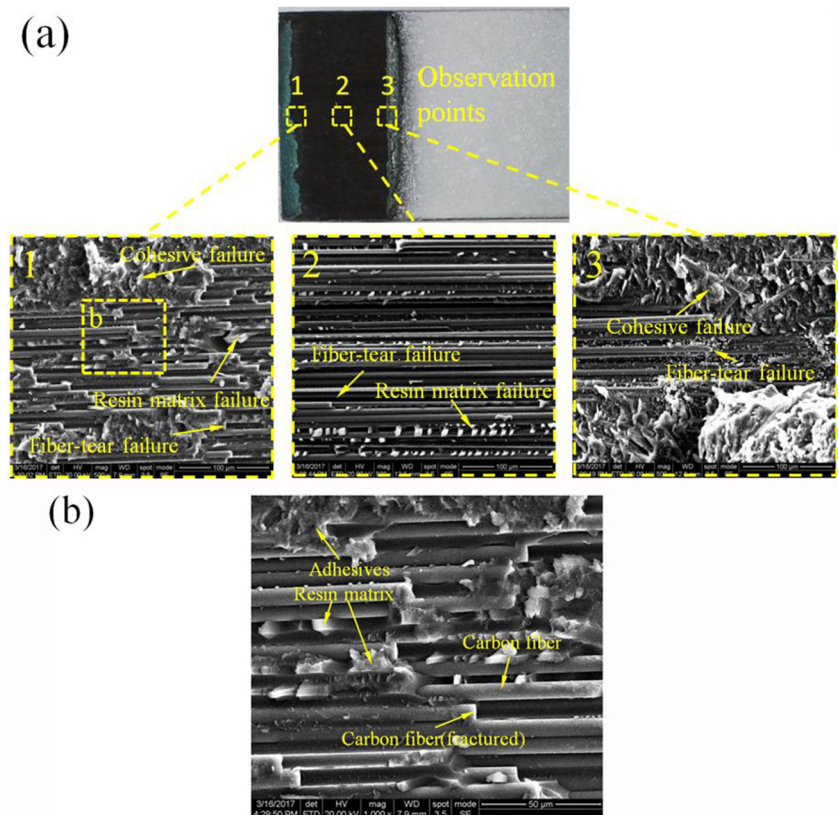
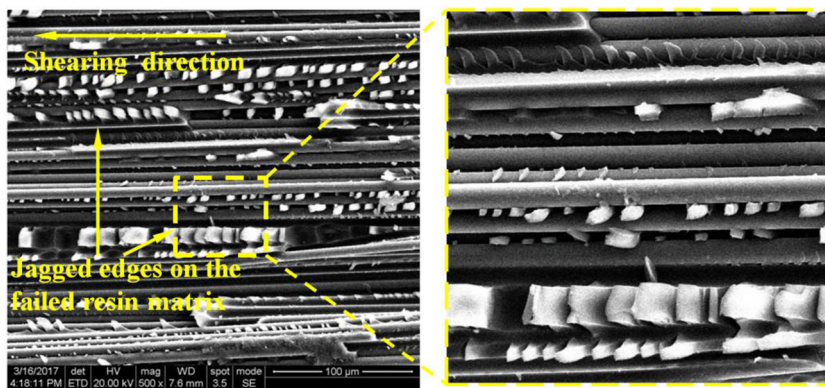


Fig. 9 Jagged edges on the failed resin matrix



area proportion of Region 1 increased with the increase of loading rate. There was no significant change in the area proportion of Region 3. But in the quasi-static shearing tests, the proportion of each area was different. The area proportion of Region 1 in any high-speed shearing tests was smaller than that of Region 1 in quasi-static shearing tests.

In the high-speed shearing tests, the area proportion was affected by loading rate and failure load. When the load reached the Peak B, cracks generated inside the adhesive joint, brittle fracture occurred, and the joint eventually failed. Due to the higher shearing rate, the failure load of the joint was larger, and the first failed region (Region 1) needed to withstand a

Fig. 10 The failure behavior partition of the joints at various loading rates

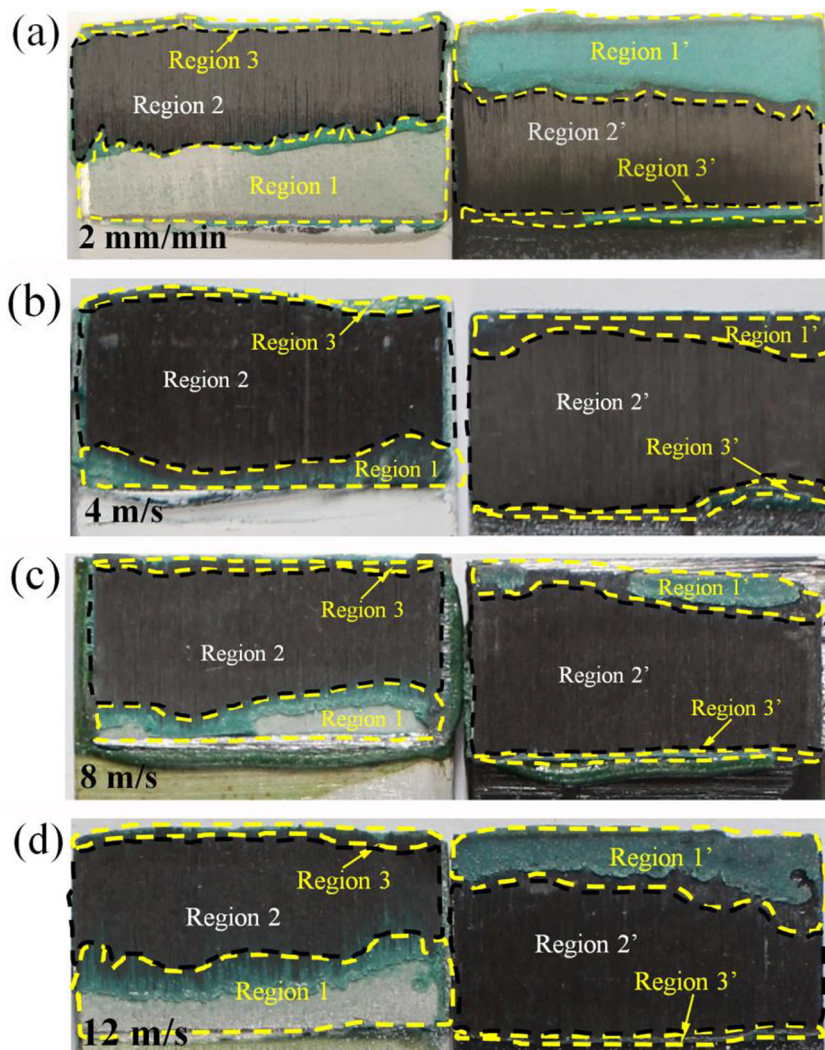


Table 5 The area proportion of Region 1 and Region 3

Loading rate	Area proportion of Region 1 (%)	Area proportion of Region 3 (%)
2 mm/min	40	<2
4 m/s	10~13	<2
8 m/s	20	<2
12 m/s	25~32	<2

higher load. As a consequence, the proportion of the cohesive failure of the adhesive was greater (namely a larger Region 1).

From Fig. 10(a), the area proportion of various regions of the quasi-static shearing tests was completely different from that of the high-speed shearing tests. And the proportion of the cohesive failure of the adhesive was higher in the quasi-static shearing tests. This phenomenon was mainly caused by the different durations of crack propagation. The duration of the joint failure process was much longer in the quasi-static shearing tests. The micro-cracks had enough time to extend in the adhesive and CFRP resin matrix. The full extension of the micro-cracks reduced the maximum load that the adhesive could withstand. Although the proportion of adhesive cohesive failure was greater in the quasi-static shearing tests, due to the sufficient extension of the micro-cracks, there were many defects in the adhesive, and the strength was degraded. Hence, the maximum load that the joint in the quasi-static shearing tests could bear was lower than that of the joint in high-speed shearing tests.

3.3 Adhesive joint failure mechanism

Based on the failure behavior analysis of the joints, it could be found that the failure mode of the joint was not symmetric along the center of the bonding area. One side was mainly the adhesive cohesive failure, and the other side was mainly the CFRP failure. This phenomenon indicated that the crack propagation of the joint was asymmetric, that is, the crack was not generated simultaneously from both ends of the bonding area and propagated to the middle of the bonding area. In order to find out the failure process and failure mechanism of the adhesive joints, the full field strain distribution was analyzed.

Figure 11(a) shows the force-displacement curves and the displacement of each peak of the joints in the high-speed shearing rates. Figure 11(b)–(d) shows strain contours of the joints at different displacement points in the high-speed shearing rates. It could be observed that the difference of the strain field distribution of the joints was not large at different shearing rates. The distribution of the strain at both ends of the bonding area was large and the distribution in the middle area was small. But the maximum strain values had certain

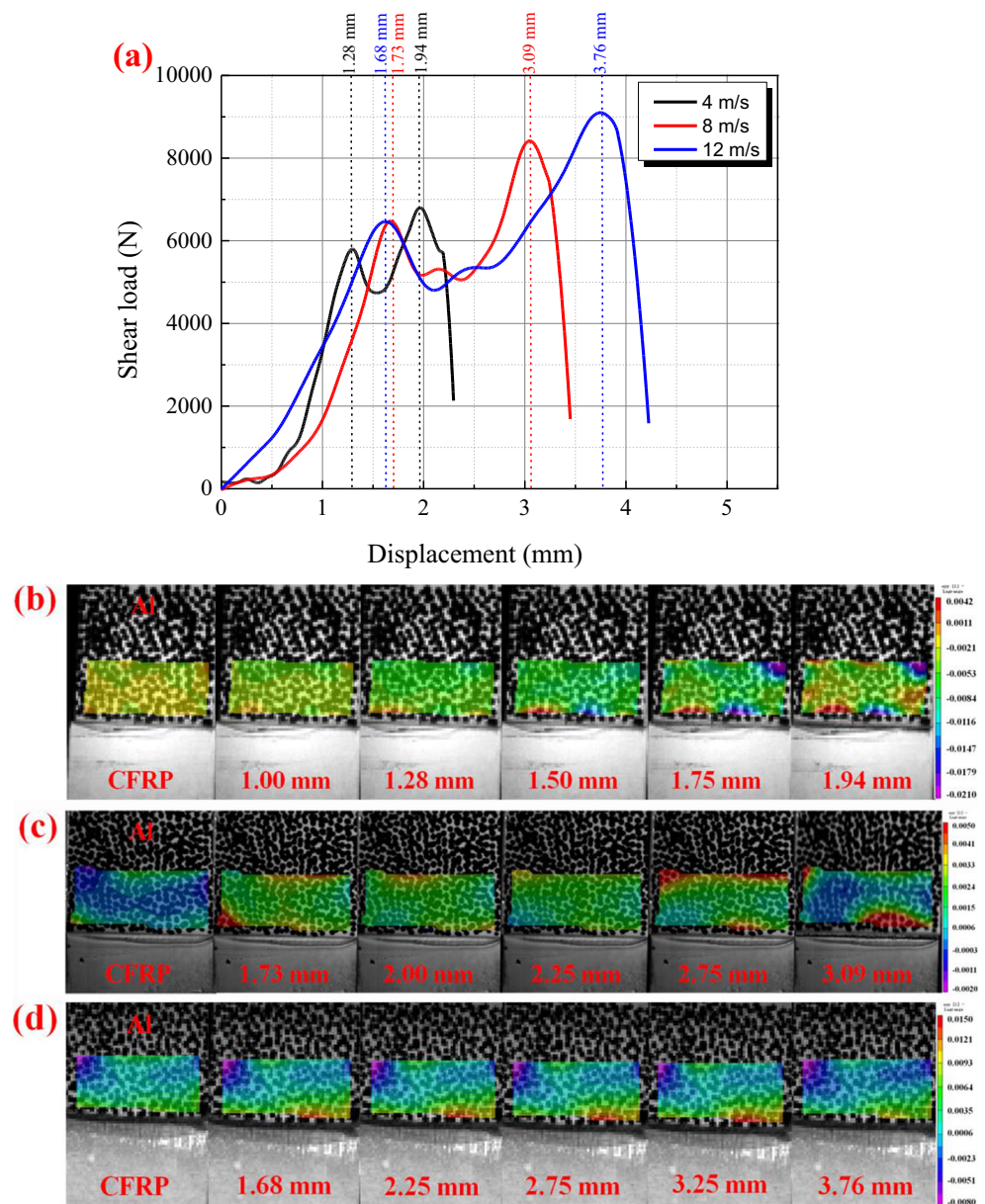
differences. The strain field of the bonding area was uniform at the beginning stage of the shearing tests. As the load increased, the stress and strain also increased. The strain field distribution of the three regions was also gradually changed in the shearing process. For Al5182 and CFRP plates, the stress and strain were a positive correlation during the shearing process. The strain increased as the stress increased. At both ends of the bonding area (the uppermost and lowermost parts of the strain contours), the strain (ϵ_{yy}) kept rising in the early stage of the loading process. The stress values were also higher at both ends of the bonding area during the shearing process. The strain of Region 1 first reached the maximum value, and then the strain of Region 3 reached the maximum value when the joint finally failed. The maximum strain was found at both ends of the bonding area (Region 1 and Region 3). However, there were some differences of the strain distribution of the bonding area at different loading rates, which was caused by the difference in the deformation of the joints during the shearing process.

In the analysis of strain field, the bonding area which was close to the side of the Al5182 plate (Region 1) deformed earlier than the other side which was near the side of the CFRP plate (Region 3). Similarly, the strain of Region 1 rose to the maximum value earlier than that of Region 3, which was caused by the failure process of the joints as shown in Fig. 12. Since the two plates (CFRP and Al5182) were not precisely collinear in the process of deformation, a torque appeared on the account of the unaligned pulling forces of the two plates in the tension process, which resulted in a bending in the joints as shown in Fig. 12(b) and (c). What's more, the Al5182 plate was easily deformed whereas the CFRP plate was not easy to deformation. Under the influence of torque, the Al5182 plate was plastically deformed, and the bonding area near the side of the Al5182 plate (Region 1) had warped deformation. The adhesive was also difficult to deform. When the Al5182 plate warped deformation, the adhesive was subjected to both the shearing and peeling forces, which made it easier to be peeled off to cause cracks and then failed (the cohesion failure). Therefore, the cracks generated first in Region 1 due to stress concentration and large warpage deformation of the Al5182 plate.

Then the adhesive joint continued to be stretched and deformed by the combination of the shearing and peeling force. Due to the low strength of the CFRP resin matrix, the cracks spread rapidly in the carbon fiber, and the surface of the CFRP plate was peeled off in Region 2 (the resin matrix failure).

Finally, at the bonding area near the side of the CFRP plate (Region 3), since the CFRP plate was hard to be deformed, the adhesive was subjected to a much smaller peeling force and failed more slowly. Thus, during the loading process, the cracks finally appeared in Region 3 and caused a small proportion of the cohesion failure of the adhesive.

Fig. 11 The strain contours of the joints at different displacements in the high-speed shearing rates: **a** displacement of the peaks; **b** strain fields evolution (4 m/s); **c** strain fields evolution (8 m/s); **d** strain fields evolution (12 m/s)



Therefore, the failure sequence of the CFRP/AI5182 single-lap adhesive joint was Region 1-Region 2-Region 3, which was consistent with the results of the full field strain analysis.

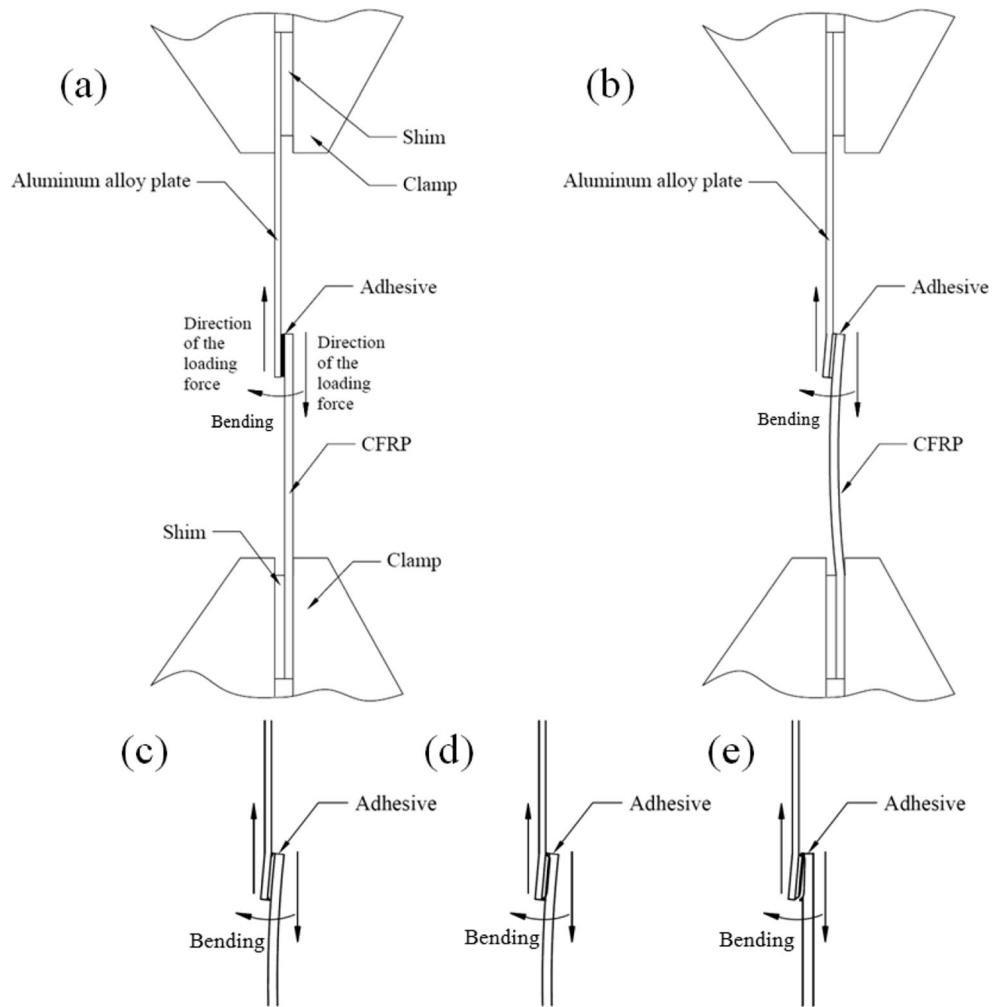
The failure analysis schematic diagram of the CFRP/AI5182 single-lap adhesive joint is shown in Fig. 13. The failure load curve could be divided into three stages. The failure modes mainly included the cohesive failure, the fiber-tear failure, and the resin matrix failure. The bonding area could be divided into Region 1, Region 2, and Region 3. The Peak A and Peak B corresponded to Region 1 and Region 3, respectively. The sequence of joint failure processes was from Region 1 to Region 2 to Region 3. The cohesive failure and the fiber-tear failure were occurred in Region 1 and

Region 3 due to the phenomenon of stress concentration. Wherein the fiber-tear failure mainly happened at the junction near Region 2. Because of the weaker strength of the CFRP resin matrix compared to the strength of the adhesive, the CFRP resin matrix failure occurred in Region 2. The cracks originated in Region 1 at first, and then propagated to Region 2, Region 3, and eventually the joint failed.

4 Conclusions

In this study, the effects of high loading rates on mechanical property, failure mode, and microscopic failure mechanism of

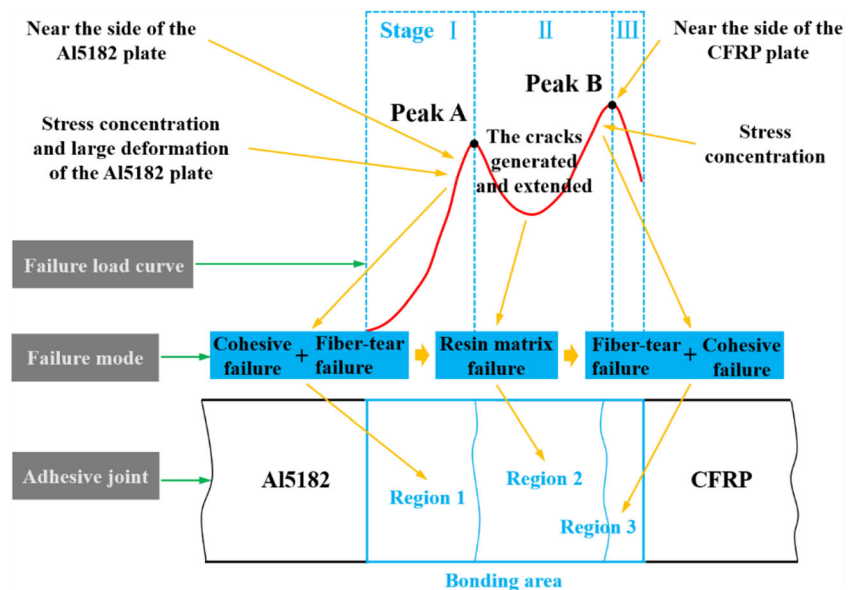
Fig. 12 The schematic diagram of the failure process: **a** specimen assembly method; **b** deformed under the influence of torque; **c** deformed of the joint; **d** cracks generated and propagated; **e** joint failed



the CFRP/Al5182 single-lap adhesive joints were investigated. The conclusions were drawn as follows:

1. The loading rate had a significant influence on the shear strength and the stiffness of the CFRP/Al5182 single-lap

Fig. 13 Failure analysis schematic diagram of the adhesive joint



adhesive joints. The shear strength and the stiffness of the joint increased with the increase of the loading rate. When the loading rate increased from 2 mm/min to 12 m/s, the average shear strength of the joint increased from 19.3 to 29.2 MPa.

2. The CFRP/A15182 single-lap adhesive joints had the similar failure behavior mode under various loading rates. At both ends of the bonding area, the failure mode was mainly cohesive failure and fiber-tear failure. At the middle of the bonding area, the failure mode was mainly resin matrix failure. Wherein the fiber-tear failure mainly occurred at the junction of the cohesive failure and the resin matrix failure.
3. According to the failure mode and location, the failure surface (the bonding area) of the adhesive joints could be divided into three regions. And the area proportion of each failure mode was different at various loading rates. There was a largest proportion of the cohesive failure of the adhesive in the quasi-static condition.
4. The full field strain analysis showed that the strain values varied greatly at both ends of the bonding area due to stress concentration. The plastic deformation of A15182 plate would occur under the influence of torque during the shearing process, which led to the adhesive being more susceptible to failure. The cracks firstly generated at one end of the adhesive joint (Region 1) and extend rapidly until the joint completely failed.
5. Peak A and Peak B corresponded to Region 1 and Region 3, respectively. The sequence of the CFRP/A15182 single-lap adhesive joints failure processes was from Region 1 to Region 2 to Region 3.

Funding information This project is supported by the Foundation for Innovative Research Groups of the National Natural Science Foundation of China (No. 51621004), National Natural Science Foundation of China (No. 51975202), the National Science Foundation of Hunan Province (2019JJ30005), and the National Key Research and Development Program of Hunan Province (2017GK2090).

Data availability The raw/processed data required to reproduce these findings cannot be shared at this time due to technical or time limitations.

Compliance with ethical standards

Conflict of interest The authors declare that they have no conflict of interest.

References

1. Mohee FM, Al-Mayah A, Plumtree A (2016) Anchors for CFRP plates: state-of-the-art review and future potential. *Compos B Eng* 90:432–442. <https://doi.org/10.1016/j.compositesb.2016.01.011>
2. Lin PC, Lin JW, Li GX (2018) Clinching process for aluminum alloy and carbon fiber-reinforced thermoplastic sheets. *Int J Adv Manuf Technol* 97:529–541. <https://doi.org/10.1007/s00170-018-1960-7>
3. Peng D, Liu Q, Li G, Cui J (2019) Investigation on hybrid joining of aluminum alloy sheets: magnetic pulse weld bonding. *Int J Adv Manuf Technol* 104:1–10. <https://doi.org/10.1007/s00170-019-04215-x>
4. Calabrese L, Galtieri G, Borsellino C, Di Bella G, Proverbio E (2016) Durability of hybrid clinch-bonded steel/aluminum joints in salt spray environment. *Int J Adv Manuf Technol* 87:3137–3147. <https://doi.org/10.1007/s00170-016-8701-6>
5. Liu X, Shao X, Li Q, Sun G (2019) Failure mechanisms in carbon fiber reinforced plastics (CFRP) / aluminum (Al) adhesive bonds subjected to low-velocity transverse pre-impact following by axial post-tension. *Compos B Eng* 172:339–351. <https://doi.org/10.1016/j.compositesb.2019.04.036>
6. Cui J, Li Y, Liu Q, Zhang X, Xu Z, Li G (2019) Joining of tubular carbon fiber-reinforced plastic/aluminum by magnetic pulse welding. *J Mater Process Technol* 264:273–282. <https://doi.org/10.1016/j.jmatprotec.2018.09.018>
7. Cui J, Dong D, Zhang X, Huang X, Lu G, Jiang H, Li G (2018) Influence of thickness of composite layers on failure behaviors of carbon fiber reinforced plastics/aluminum alloy electromagnetic riveted lap joints under high-speed loading. *Int J Impact Eng* 115: 1–9. <https://doi.org/10.1016/j.ijimpeng.2018.01.004>
8. Pramanik A, Basak AK, Dong Y, Sarker PK, Uddin MS, Littlefair G, Dixit AR, Chattopadhyaya S (2017) Joining of carbon fibre reinforced polymer (CFRP) composites and aluminium alloys—a review. *Compos A Appl Sci Manuf* 101:1–29. <https://doi.org/10.1016/j.compositesa.2017.06.007>
9. Sun G, Liu X, Zheng G, Gong Z, Li Q (2018) On fracture characteristics of adhesive joints with dissimilar materials—an experimental study using digital image correlation (DIC) technique. *Compos Struct* 201:1056–1075. <https://doi.org/10.1016/j.compstruct.2018.06.018>
10. Li Y, Zhan X, Gao C, Wang H, Yang Y (2019) Comparative study of infrared laser surface treatment and ultraviolet laser surface treatment of CFRP laminates. *Int J Adv Manuf Technol* 102(9):4059–4071. <https://doi.org/10.1007/s00170-019-03368-z>
11. Pizzorni M, Lertora E, Gambaro C, Mandolfino C, Salerno M, Prato M (2019) Low-pressure plasma treatment of CFRP substrates for epoxy-adhesive bonding: an investigation of the effect of various process gases. *Int J Adv Manuf Technol* 102(9):3021–3035. <https://doi.org/10.1007/s00170-019-03350-9>
12. Fortunato J, Anand C, Braga DFO, Groves RM, Moreira PMGP, Infante V (2017) Friction stir weld-bonding defect inspection using phased array ultrasonic testing. *Int J Adv Manuf Technol* 93(9–12): 3125–3134. <https://doi.org/10.1007/s00170-017-0770-7>
13. Machado JJM, Marques EAS, da Silva LFM (2017) Adhesives and adhesive joints under impact loadings: an overview. *J Adhes*:1–32. <https://doi.org/10.1080/00218464.2017.1282349>
14. Araújo HAM, Machado JJM, Marques EAS, da Silva LFM (2017) Dynamic behaviour of composite adhesive joints for the automotive industry. *Compos Struct* 171:549–561. <https://doi.org/10.1016/j.compstruct.2017.03.071>
15. Machado JJM, Marques EAS, da Silva LFM (2018) Influence of low and high temperature on mixed adhesive joints under quasi-static and impact conditions. *Compos Struct* 194:68–79. <https://doi.org/10.1016/j.compstruct.2018.03.093>
16. Machado JJM, Nunes PDP, Marques EAS, da Silva LFM (2019) Adhesive joints using aluminium and CFRP substrates tested at low and high temperatures under quasi-static and impact conditions for the automotive industry. *Compos B Eng* 158:102–116. <https://doi.org/10.1016/j.compositesb.2018.09.067>
17. Srivastava V, Parameswaran V, Shukla A, Morgan D (2002) Effect of loading rate and geometry variation on the dynamic shear strength of adhesive lap joints. In: Gdoutos E.E. (eds) *Recent*

- Advances in Experimental Mechanics. Springer, Dordrecht. https://doi.org/10.1007/0-306-48410-2_71
18. Liu X, Shao X, Li Q, Sun G (2019) Experimental study on residual properties of carbon fibre reinforced plastic (CFRP) and aluminum single-lap adhesive joints at different strain rates after transverse pre-impact. *Compos A Appl Sci Manuf* 124:105372. <https://doi.org/10.1016/j.compositesa.2019.03.018>
 19. ISO 4587 (2003) Adhesives — determination of tensile lap-shear strength of rigid-to-rigid bonded assemblies
 20. Naito K, Onta M, Kogo Y (2012) The effect of adhesive thickness on tensile and shear strength of polyimide adhesive. *Int J Adhes Adhes* 36:77–85. <https://doi.org/10.1016/j.ijadhadh.2012.03.007>
 21. Boutar Y, Naïmi S, Mezlini S, Carbas RJC, da Silva LFM, Ben Sik Ali M (2018) Fatigue resistance of an aluminium one-component polyurethane adhesive joint for the automotive industry: effect of surface roughness and adhesive thickness. *Int J Adhes Adhes* 83: 143–152. <https://doi.org/10.1016/j.ijadhadh.2018.02.012>
 22. Al-Mosawe A, Al-Mahaidi R, Zhao X-L (2016) Bond behaviour between CFRP laminates and steel members under different loading rates. *Compos Struct* 148:236–251. <https://doi.org/10.1016/j.compstruct.2016.04.002>
 23. Jia Z, Hui D, Yuan G, Lair J, Lau K-t XF (2016) Mechanical properties of an epoxy-based adhesive under high strain rate loadings at low temperature environment. *Compos B Eng* 105:132–137. <https://doi.org/10.1016/j.compositesb.2016.08.034>
 24. He J, Xian G (2016) Debonding of CFRP-to-steel joints with CFRP delamination. *Compos Struct* 153:12–20. <https://doi.org/10.1016/j.compstruct.2016.05.100>

Publisher's note Springer Nature remains neutral with regard to jurisdictional claims in published maps and institutional affiliations.